

## Macroscopic Stability of High $\beta_N$ MAST Plasmas

I.T. Chapman 1), R.J. Akers 1), L.C. Appel 1), N.C. Barratt 2), M.F. de Bock 1,7), A.R. Field 1), K.J. Gibson 2), M.P. Gryaznevich 1), R.J. Hastie 1), T.C. Hender 1), D.F. Howell 1), M.-D. Hua 1,3), G. Huysmans 4), Y.Q. Liu 1), C. Michael 1), G. Naylor 1), T. O’Gorman 1,5), S.D. Pinches 1), R. Scannell 1), S.A. Sabbagh 6), H.R. Wilson 2) and the MAST Team

1) Euratom/CCFE Fusion Association, Culham Science Centre, Abingdon, OX14 3DB, UK

2) Department of Physics, University of York, Heslington, York, UK

3) Imperial College, Prince Consort Road, London, SW7 2BY, UK

4) CEA-Cadarache, Association Euratom-CEA, 13108 St Paul-lez-Durance, France

5) Department of Electrical and Electronic Engineering, University College Cork, Ireland

6) Dept of Applied Physics and Applied Maths, Columbia University, New York, NY, USA

7) Technische Universiteit Eindhoven, Den Dolech 2, P.O. Box 513, Eindhoven, Netherlands

e-mail contact of main author: [ian.chapman@ccfe.ac.uk](mailto:ian.chapman@ccfe.ac.uk)

**Abstract.** The high-beta capability of the spherical tokamak geometry, coupled with a suite of world-leading diagnostics on MAST, has facilitated significant improvements in the understanding of performance limiting core instabilities in high  $\beta_N$  plasmas. The saturated LLM was diagnosed as an ideal internal mode growing unstable as  $q_{min}$  approaches one and incurring rotation damping predicted by NTV theory. NTM critical island width physics has been addressed by  $< 1$ cm resolution TS measurements and RWM stability limits have been probed by MHD spectroscopy and state-of-the-art numerical modelling.

### 1. Introduction

In order to achieve steady-state burning plasmas it is necessary to maximise the triple product  $nT\tau_E = \beta\tau_E B^2$  where  $\beta$  is the ratio of plasma energy to magnetic field energy,  $n, T, p$  are the plasma density, temperature and pressure respectively,  $\tau_E$  is the energy confinement time and  $B$  is the toroidal magnetic field. The spherical tokamak maximises  $\beta$  by optimising the magnetic topology. Simultaneously, it is necessary to minimise the amount of power required to supply the current non-inductively. ‘Advanced tokamak’ (AT) scenarios [1] aim to maximise the bootstrap current by operating at high plasma pressure and low plasma current. However, the energy confinement degrades with decreasing plasma current, so in order to operate at most attractive fusion performance, the  $\beta$  must be optimised. However, operating at increased pressure and low current can exacerbate MHD instabilities, such as resistive wall modes (RWMs), neoclassical tearing modes (NTMs), and saturated long-lived modes (LLMs). Recent MAST experiments, coupled with sophisticated modelling of plasma stability, have focussed on improving the understanding of these instabilities and their evolution to aid future design of scenarios.

### 2. Saturated ideal instabilities in Advanced Tokamak plasmas

AT plasmas in MAST with a safety factor above unity and a  $q$ -profile with either weakly reversed shear, or broad low shear regions (as illustrated in figure 1a) regularly exhibit long-lived saturated ideal MHD instabilities [2]. Such MAST discharges exhibit frequency sweeping  $n = 1$  modes that evolve into a saturated mode (figure 1b) whose frequency evolution is close to that of the central rotation measured by charge exchange recombination spectroscopy. These ideal modes, distinguished as such by the notable lack of islands or signs of reconnection, are driven unstable as the safety factor approaches unity. In the presence of such ideal perturbations, the toroidal rotation profile is flattened and the fast ion losses are enhanced.

Theory analysing reversed shear  $q$  profiles indicates that they are prone to the  $(m, n) = (1, 1)$

internal kink mode [3]. Simulation of Soft X-ray (SXR) fluctuations show that the eigenstructure of the LLM is consistent with that of an  $(m, n) = (1, 1)$  internal kink mode. The mode is unstable, even at zero  $\beta$ , for  $\Delta q = q_{min} - 1$  under a critical value  $\Delta q_{crit}$  [3]. In low toroidal field discharges, the entire  $q$  profile was lower and  $\Delta q$  approached zero earlier than in high field discharges. The onset of the LLM was consistently observed earlier despite lower  $\beta$ , which suggests a  $\Delta q$  threshold for the triggering of the mode. This mode saturates non-linearly if the  $q$  profile remains above 1 [4]. Since the mode is ideal, the saturation occurs when the stabilising field line bending term balances the mode's fluid drive. Flatter core  $q$  profiles are found to be unstable to low  $(m, n)$  internal kink-ballooning instabilities, called infernal modes [5], with the most unstable modes having  $m = n$  when  $\Delta q \sim 0$ . These modes also feature a critical value of  $\Delta q$  under which they are destabilised,  $\Delta q_{crit}$  [3]. This critical value decreases with the  $n$  number, whereas the mode's growth rate increases with it as  $q_{min} \rightarrow 1$ . Analytic stability analysis (see [2]) suggests that increasing the  $\beta$  raises susceptibility to infernal modes (since the growth rate scales with  $\beta_N^2$ ), as does widening the region of low magnetic shear (scaling with  $(r_1/R)^2$ ). Of course, in spherical tokamaks like MAST,  $\beta_p$  is naturally high and the region of low-shear is typically very large, extending well beyond mid-radius, making ST plasmas with  $q_{min} \sim 1$  particularly susceptible to ideal infernal modes.

The linear stability of the  $n = 1$  internal mode has been assessed for the evolving  $q$ -profile exhibited in MAST plasmas. The  $q$ -profile has been reconstructed for discharge 21781 by constraining the EFIT++ equilibrium reconstruction with MSE and magnetic measurements. The current profile and plasma shape are then supplied to the HELENA equilibrium code [6] together with the pressure profile shape derived from the high resolution TS measurements. The linear stability of this equilibrium is found using the CASTOR MHD code [7]. The ideal  $n = 1$  internal mode becomes unstable at approximately the same time as the LLM appears experimentally. The mode is driven unstable primarily by the decrease in  $\Delta q$  rather than an increase in plasma pressure.

The  $n = 2$  component of the experimentally observed LLM is not detected in the SXR spectrogram at LLM onset, whereas it appears and grows in amplitude as  $\Delta q$  decreases. Whilst the  $n > 1$  modes arise as a nonlinear consequence of the  $n = 1$  mode, the change in their relative amplitude is likely to occur because of a resonant field amplification effect [8] in the higher- $n$  harmonics as they become marginally unstable. The higher- $n$  modes become progressively more unstable at a sufficiently small  $\Delta q$ . It is possible to infer from figure 1c that as  $q_{min}$  drops, the plasma first becomes unstable to the  $n = 1$  kink mode, as observed experimentally. As the current continues to diffuse and the safety factor drops, the  $n = 2$  mode becomes marginally unstable. As this time point is approached, the weakly damped  $n = 2$  mode will resonantly amplify the  $n = 2$  harmonics resulting nonlinearly from the  $n = 1$  LLM. This appears to be in excellent agreement with the empirical observations and analytic calculations [9] which suggest that for very broad low-shear regions present in these MAST discharges as  $q_{min} \rightarrow 1$ , the higher- $n$  infernal modes become more unstable than the  $n = 1$  harmonic.

Finally, the transition from the chirping modes to the saturated mode can also be explained by the safety factor evolution. The fishbone dispersion relation [10] recast for equilibria with non-monotonic  $q$ -profiles becomes [2]

$$\delta\hat{W}_f + \sqrt{r_1^2 q''} \left[ (\Delta q)^2 - 3\Omega(\Omega - \Omega_{*pi}) \left( \frac{\bar{\omega}_{dm}^2}{\omega_A^2} \right) \right]^{1/2} \left[ \Delta q + \left( (\Delta q)^2 - 3\Omega(\Omega - \Omega_{*pi}) \frac{\bar{\omega}_{dm}^2}{\omega_A^2} \right)^{1/2} \right]^{1/2} + \langle \beta_h \hat{I}_0 \rangle \Omega \log \left( 1 - \frac{1}{\Omega} \right) = 0 \quad (1)$$

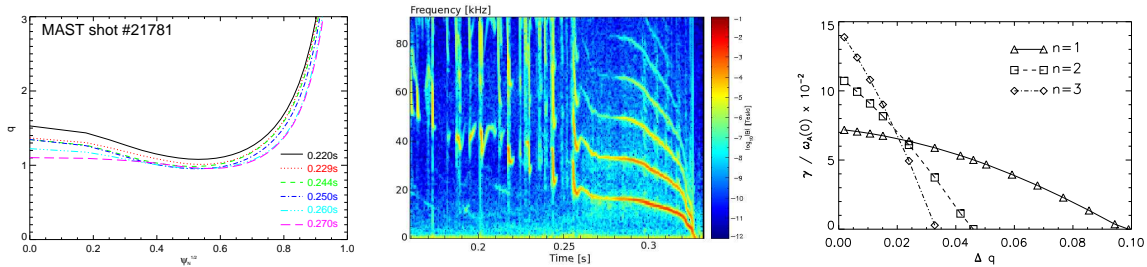


FIG. 1. (left) The  $q$ -profile evolution in MAST shot 21781 for different time (in s); (centre) The Fourier spectrogram of outboard midplane magnetic measurements showing chirping modes which transition into a long-living saturated mode; (right) The growth rate of the  $n = 1, 2, 3$  modes as a function of  $\Delta q$  found by MISHKA.

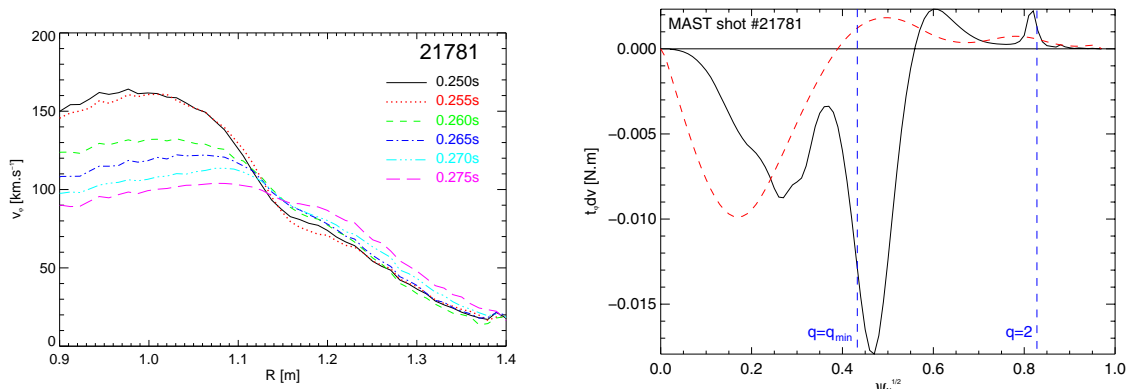


FIG. 2. (left) The rotation profile in MAST shot 21781 exhibiting strong braking after LLM onset at 255ms; (right) The measured torque compared to the predicted NTV torque showing good agreement.

where  $\Omega = \omega / \bar{\omega}_{dm}$ ,  $\bar{\omega}_{dm} = \bar{\omega}_{dh}(E = E_m)$ ,  $\bar{\omega}_{dh}$  is the toroidal precession frequency of the trapped energetic particles,  $E_m$  is the upper bound of the energy range of the fast ion distribution,  $\beta_h$  is the fast ion beta,  $\Omega_{*pi}$  is the ion diamagnetic frequency and  $\hat{I}_0$  is defined in reference [10]. For fishbones to be unstable in plasmas with a monotonic  $q$ -profile, the  $\beta_h$  term must be sufficiently large as to overcome the Alfvén continuum damping around the  $q = 1$  surface. However, in reversed shear plasmas, the continuum damping can be eliminated without the  $\omega_{*pi}$  diamagnetic terms to produce a continuum gap. Indeed if  $\Delta q > 0$ , the continuum gap is in the range  $[-\Delta q \omega_A / \sqrt{3}, +\Delta q \omega_A / \sqrt{3}]$ . For fishbones to be unstable  $\Delta q < \Delta q_{crit,f} > \Delta q_{crit}$ . The fact that fishbones would be unstable at a larger  $\Delta q$  than required for the LLM to become unstable agrees well with the behaviour exhibited experimentally as the safety factor evolves. It is conjectured that once  $\Delta q < \Delta q_{crit}$  and the LLM becomes unstable, the enhanced fast ion losses associated with the mode mean that there are no longer sufficient energetic ions within the core of the plasma to drive the fishbones, and the chirping activity ceases.

### 3. Rotation braking

Following the onset of the LLM, the mode's rotation frequency remains constant while that of the plasma core is rapidly damped (figure 2(left)). After this phase, both rotation frequencies gradually decrease, probably due to mode locking. Whilst electromagnetic torques can appear even in the absence of magnetic reconnection [11], they are localised around integer  $q$  positions, which are located outside the region of observed rotation damping. These torques may account for the slight edge rotation acceleration, but they cannot explain the core damping, as MAST momentum confinement times ( $\sim 50$ ms) do not allow such localised slowing down to diffuse into the core on the observed timescales ( $\sim 5$ ms). In contrast, the distributed, fast

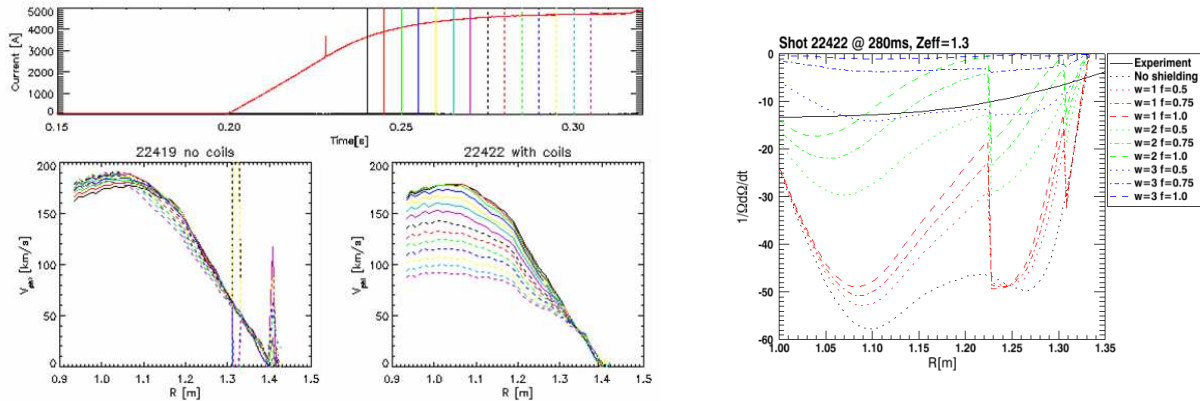


FIG. 3. (left) The rotation profile in MAST shot 22422 exhibiting strong braking when an  $n = 2$  external field is applied; (right) The measured rate of change of angular momentum compared to predicted NTV torque for different assumptions of plasma screening.

damping mechanism of Neoclassical Toroidal Viscosity (NTV) theory [12], arising from the non-axisymmetry of the magnetic field, seems well suited to account for the observed braking. This theory can be used if the field's axisymmetry is broken, in this case by the presence of an MHD instability, whereby the torque arises from the differential flow of the plasma through the non-axisymmetric perturbation. In this case, the flow damping brings the rotation of the plasma into agreement with that of the magnetic structure. The eigenstructure of the mode was calculated using the CASTOR code [7], and its saturated amplitude estimated by comparing experimental SXR data to simulations for different eigenstructure amplitudes. The structure of the magnetic perturbation obtained was then used to estimate the NTV torque in the  $1/\nu$  regime for shot 21781 at  $t = 255$ ms according to reference [13]. Except at the  $q_{min}$  location and rational surfaces, the results show strong similarities with the measured rate of change of the angular momentum density (figure 2(right)). Here, the changes to the mode's eigenstructure as it saturates, likely to be small [4], and the effect of enhanced fast ion losses are neglected.

External magnetic perturbations have also been applied in co- and counter-NBI heated plasmas to further test NTV theory. Non-axisymmetric  $n = 2$  fields have been applied from MAST's in-vessel coils – constituting two rows of six coils equally spaced and symmetric above and below the midplane – and braking measured with CXRS. The damping observed in a counter-NBI plasma is compared to the predicted torque arising from NTV theory in figure 3. There is a factor of five discrepancy between experiment and theory, though by reducing the resonant component for  $w$  harmonics around a given resonant surface by a factor of  $f$  (where 1 is complete plasma shielding) the agreement is improved, suggesting a strong plasma shielding of the resonant torque. Further modelling to include the plasma response rigorously (which is implicitly included in the simulations of braking from the LLM) will be undertaken with MARS [20]. Future experiments will attempt to develop MHD-quiescent comparison co-NBI plasmas in order to assess the neoclassical offset term expected from theory and scan ion collisionality to test NTV theory in lower collisionality regimes relevant to ITER.

#### 4. Resistive Wall Mode Physics

The broad current profile and peaked pressure profile of reversed shear scenarios also make them prone to RWMs. However, operation above the stability limit for RWM onset is important in order to achieve economically-attractive plasma performance in advanced tokamak regimes. Various experiments have shown that the plasma can operate above the no-wall  $\beta$ -limit, even with very low rotation [14, 15]. Consequently, there is a need to understand the passive stabili-

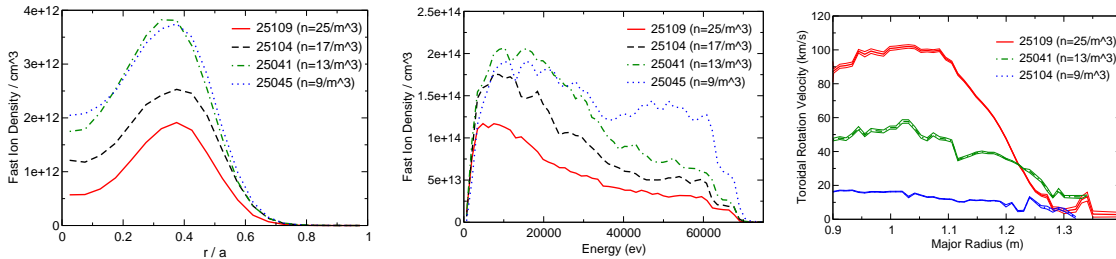


FIG. 4. The fast ion density with respect to (left) radius and (centre) energy as predicted by TRANSP [28] and (right) the rotation profile measured by the CXRS for MAST discharges 25109 ( $\bar{n}_e = 25 \times 10^{18} m^{-3}$ ), 25104 ( $\bar{n}_e = 17 \times 10^{18} m^{-3}$ ), 25041 ( $\bar{n}_e = 13 \times 10^{18} m^{-3}$ ) and 25045 ( $\bar{n}_e = 9 \times 10^{18} m^{-3}$ ).

sation occurring from kinetic effects which is thought to underlie these results. Various models have been presented to explain the RWM damping due to kinetic effects, such as sound-wave damping [16], ion Landau damping [17], or the precessional drift resonance with thermal ions [18]. Numerical simulation has shown that the damping from resonance with  $\omega_d$  of thermal ions [19, 20, 21] and fast ions [22, 23] can significantly raise the RWM stability limit.

One way to probe RWM stability experimentally is to examine the plasma response to externally applied non-axisymmetric magnetic fields [24]. When the plasma pressure exceeds the no-wall  $\beta$ -limit, strong resonant field amplification (RFA) occurs [25]. In MAST,  $n = 1$  oscillating non-axisymmetric fields are applied from internal coils with frequency from 30 to 100Hz. By measuring the plasma response on saddle loops, both in the same sector as the internal coils applying the perturbation and in orthogonal sectors, the RFA is defined as  $A_{RFA} = (B_r(r_{sensor}) - B_r^{ext})/B_r^{ext}$ . Fitting the RFA frequency spectrum allows the effective mutual inductance and RWM growth rate in the absence of applied fields to be found according to a single mode model in reference [25], allowing the plasma response at the wall to be found.

MAST plasmas have operated well above the ideal no-wall limit predicted by the RFA limit or from linear stability analysis (where rigorous equilibrium reconstruction has been shown to be highly accurate in the LLM onset studies in section 2). In order to test whether significant damping is caused by the NBI fast ions, the plasma response has been measured for a range of fast ion distributions – achieved by varying plasma density – and compared to the damping rate [18]:  $\gamma\tau_W = -(\delta W_\infty + \delta W_K)/(\delta W_b + \delta W_K)$  where  $\delta W_{b,\infty}$  represents the sum of the plasma and vacuum energy with and without a wall (here comprising the poloidal field coil casings and other toroidally continuous conducting structures) respectively calculated using MISHKA-1 [26] and  $\delta W_K$  is the kinetic contribution to the plasma energy calculated using HAGIS, a Monte-Carlo drift kinetic code [27] which includes finite orbit width effects. By vertically displacing the plasma downwards, the neutral beam deposition was shifted off-axis, avoiding the strongly stabilising effect of a fast ion population peaked on-axis leading to large disruptive sawteeth. This permitted access to high  $\beta_N$ , and the small regular sawteeth mediate approximately constant  $q$ -profiles despite significant changes in the density. Increasing the density results in the fast ion distribution becoming peaked further off-axis and at lower energies, as well as increasing the plasma rotation, as illustrated in figure 4. By scanning the plasma density the toroidal rotation is varied such that  $v_0/v_A \in [0.01, 0.10]$  and the fast particle fraction is in the range  $\beta_h/\beta_{tot} \in [0.09, 0.60]$ . The fast ion radial excursion remains approximately constant ( $\Delta/a \approx 0.2$  which can play a significant role in spherical tokamaks); this is not the case if  $I_p/B_t$  is changed in order to change fast ion density whilst keeping  $q$  the same [22].

Both rotation and kinetic effects contribute to allowing operation well above the ideal no-wall limit, and the two effects are intricately related. The change in the potential energy of the

mode due to kinetic effects,  $\delta W_K$  incorporates a frequency resonance condition [19, 20, 22] with either the transit frequency of passing particles,  $\omega - \omega_E \sim \omega_t \sim v/R$ ; the bounce frequency of the trapped particles,  $\omega - \omega_E \sim \omega_b \sim \sqrt{r/R}(v/R)$ ; or the precession drift motion,  $\omega - \omega_E \sim \omega_d \sim \rho/r(v/R)$ , where  $\omega_d \ll \omega_b < \omega_t$  and  $\rho$  is the Larmor radius,  $\rho = mv_\perp/eB$  and  $v_\perp$  is the particle speed perpendicular to the magnetic field. Whilst it has been shown that the low-frequency RWM can resonate with both the precession drift frequency and bounce frequencies of thermal ions (depending on the plasma rotation) [19, 21, 20], for energetic particles typically  $\omega_d, \omega_b \gg \omega - \omega_E$ . Consequently, it is likely that the contribution from the energetic particles is not a resonant process, but related to (i) an increase in the resistance to changes in the magnetic flux by the kink mode through an inhibition of toroidal coupling of harmonics and (ii) finite orbit width effects of the energetic ions.

In order to explicate the role of the beam ions in damping the RWM,  $\delta W_K$  has been calculated with HAGIS for MAST plasmas with different plasma densities. By using a drift kinetic code, the frequencies of all of the particles can be calculated rigorously as  $\omega_\phi = \oint \phi dt / \oint dt$  integrating around a closed poloidal orbit and  $\omega_\theta = 2\pi/\Delta t$  including the radial excursion of the orbits which are neglected in hybrid MHD eg MARS-K [20]. Whilst the particle orbits and finite radial excursion are treated comprehensively, the drift kinetic modification of the RWM eigenfunction is neglected and the eigenfunction of the ideal external kink or kink-ballooning mode produced by MISHKA is not corrected. Whilst this is usually acceptable, the perturbative approach has been shown to over-predict stability [20].

At high plasma density, the rotation is sufficiently large that the Doppler shifted mode frequency approaches the beam ion drift precession frequency. However, the low fast ion beta (where  $\delta W_K$  scales with  $\beta_h$ ) coupled with increased collisionality means that the NBI ions do not strongly damp the RWM. Conversely, at very low density, the high fast ion fraction, increased effective orbit width effects and low plasma rotation result in enhanced fast ion stabilisation. As  $v_0/v_A \rightarrow 0.01$ ,  $\omega - \omega_E$  has a strong resonance with the precession frequency of the thermal ions too, significantly increasing  $\delta W_K$ . Indeed, even though the fast ion contribution is strongest at low density, the resulting low rotation means that the thermal ion stabilisation dominates the kinetic damping of the RWM, as illustrated in figure 5. The RWM is least stable at intermediate densities, where corresponding intermediate rotation avoids resonance with either the thermal or fast ion precession frequency or the thermal bounce frequency. This is in qualitative agreement with MAST experiments, where the plasma response to the applied field is greatest at intermediate density.

The interaction between the RWM, the applied fields, the plasma rotation and other MHD instabilities is an inherently nonlinear problem. Consequently, the nonlinear behaviour of the RWM has been studied in general toroidal geometry for typical current and pressure profiles by solving the reduced MHD equations with the JOREK code [29]. In initial studies, the hot core plasma, with density  $\rho_0$  is surrounded by a cold plasma with low density,  $\rho_w$ , and high resistivity. Outside the cold plasma is a resistive wall at  $r = r_{rw} > a$  with resistivity  $\eta_w$ , which

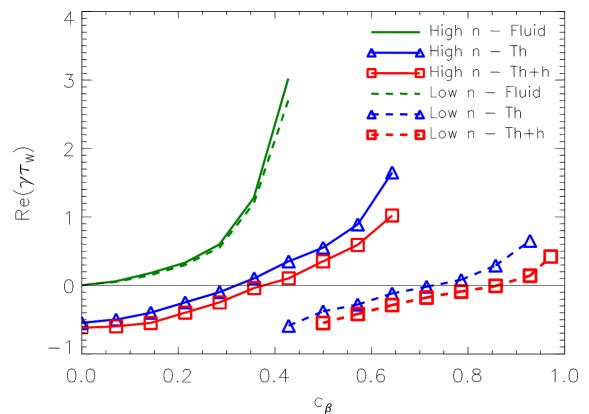


FIG. 5. The growth/damping rate of the RWM for high and low density MAST plasmas with respect to  $c_\beta = (\beta - \beta_{nowall})/(\beta_{wall} - \beta_{nowall})$ . The damping is stronger for low density. In both cases thermal kinetic effects dominate the NBI contribution.

in turn is surrounded by a vacuum and an ideal wall at  $r = r_w > r_{rw}$ . Whilst the linear growth rate of the RWM for  $r_{rw} = 1.3a$  depends upon the density of the cold temperature, high resistivity plasma surrounding the core plasma, the nonlinear saturation level does not, in good agreement with cylindrical modelling [30]. Nonlinear simulations of RWMs have also been performed at artificially inflated plasma pressure such that the equilibrium is found to be unstable to both the  $m/n = 2/1$  RWM and an internal  $3/2$  mode. Figure 6 illustrates that in the presence of the RWM, the  $3/2$  mode is significantly destabilised in the nonlinear phase, due to the change in current profile at the  $q = 3/2$  surface resulting from the growth of the  $n = 1$  mode. This example illustrates the nonlinear mode coupling which can be studied with JOREK, even using reduced MHD which neglects some important tearing mode physics. Such interaction between the RWM and other instabilities may help to shed light on recent observation of RWM coupling with fishbones [31] and ELMs [32].

### 5. Neoclassical Tearing Mode Stability

Before RWMs are encountered, NTMs often inhibit high  $\beta$  plasmas. The upgraded MAST Thomson Scattering (TS) system provides excellent spatial resolution ( $\sim 1\text{cm}$ ) at over 130 radial locations across the full plasma diameter, and utilises 8 individual lasers which can be operated in burst mode, whereby the laser separation can be adjusted to within a few microseconds. This provides detailed profiles of transient and periodic phenomena such as temperature perturbations associated with neoclassical tearing mode (NTM) islands, as illustrated in toroidal cross-section in figure 7. Using a simplified model in which finite parallel diffusive heat transport can provide a threshold for NTM island growth [33] it has been demonstrated that the TS derived electron temperature profiles around an island can be used to obtain both the island width and the critical island width below which temperature gradients are maintained across the island, potentially removing the NTM drive. Initial results from high beta discharges show that the measured island width inferred from the TS data is in good agreement with magnetic estimates of the island width (considering both a cylindrical approximation and using a full field line tracing estimate). The temporal behaviour of the island width obtained from magnetic diagnostics indicates that for the scenarios considered to date, the observed threshold island width is larger than the critical width predicted assuming finite parallel diffusive transport [34].

### 6. Conclusions

Detailed macroscopic stability studies on MAST facilitated by very high resolution diagnostics have shed new light on performance-limiting instabilities in high  $\beta$  plasmas. The saturated

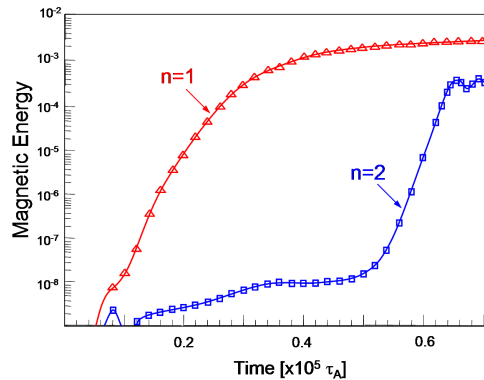


FIG. 6. Time evolution of the magnetic energy of the  $3/2$  and  $2/1$  components. The  $3/2$  mode is destabilised in the nonlinear phase.

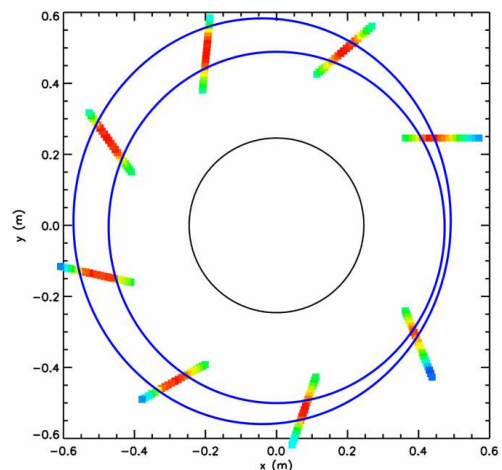


FIG. 7.  $|T - T(q = 2)|$  at an NTM island in shot 24623 showing the flattened temperature region in red and the  $n = 1$  structure identified by the extent of the flat regions in blue.

long-lived mode was diagnosed as an ideal internal mode growing unstable as  $q_{min}$  approaches one. This mode degrades confinement, expels energetic ions and induces rotation damping that is in good accordance with NTV theory, and consequently future STs must keep  $\Delta q$  above the critical threshold for mode onset, typically  $\Delta q \sim 0.1$ . The LLM saturates nonlinearly at a sufficiently large amplitude of the displacement that the stabilising field-line bending term in the ideal MHD equations will dominate and prevent further growth. NTM critical island width physics has been addressed by  $< 1\text{cm}$  resolution TS measurements which observe threshold island widths larger than the critical width predicted assuming finite parallel diffusive transport. RWM stability limits have been probed by MHD spectroscopy and state-of-the-art numerical modelling. MAST plasmas have operated to  $\beta_N = 5.7$  well above the predicted ideal no-wall limit or measured RFA limits due to a combination of rotation and kinetic damping. By varying the density, both the rotation and the fast ion distribution function have been changed dramatically. Detailed drift kinetic modelling shows that whilst the contribution of the NBI ions to RWM damping does increase at sufficiently high plasma rotation as to allow resonance with the fast ion precession frequency, the thermal ion damping always dominates over the fast ion contribution.

## References

- [1] TAYLOR T, *Plasma Phys Control Fusion* **39** (1997) B47
- [2] CHAPMAN IT *et al*, *Nucl Fusion* **50** (2010) 045007
- [3] HASTIE RJ *et al.*, *Phys. Fluids* **30** (1987) 1756
- [4] AVINASH *et al*, *Phys. Rev. Lett.* **59** (1987) 2647
- [5] MANICKAM J *et al.*, *Nucl. Fusion* **27** (1987) 1461
- [6] HUYSMANS GTA *et al*, *Proc CP90 Conf on Comp Phys* (1991) p. 371
- [7] KERNER W *et al*, *Contr. Fusion and Plas. Phys. 18th Conf. Berlin Part IV* (1991) p89
- [8] BOOZER AH, *Phys. Rev. Lett.* **86** (2001) 5059
- [9] WAHLBERG C and GRAVES JP, *Phys. Plasmas* **14** (2007) 110703
- [10] CHEN L, WHITE RB and ROSENBLUTH MN, *Phys. Rev. Lett.* **52** (1984) 1122
- [11] TAYLOR JB, *Phys. Rev. Lett.* **91** (2003) 115002
- [12] SHAING KC *et al*, *Phys. Plasmas* **10** (2003) 1443
- [13] COLE AJ *et al*, *Phys. Rev. Lett.* **99** (2007) 065001
- [14] REIMERDES H *et al*, *Phys. Rev. Lett.* **98** (2007) 055001
- [15] TAKECHI M *et al*, *Phys. Rev. Lett.* **98** (2007) 055002
- [16] BONDESON A and WARD DJ, *Phys. Rev. Lett.* **72** (1994) 2709
- [17] CHU MS *et al*, *Phys. Plasmas* **2** (1995) 2236
- [18] HU B and BETTI R, *Phys. Rev. Lett.* **93** (2004) 105002
- [19] CHAPMAN IT *et al*, *Plasma Phys Control Fusion* **51** (2009) 055015
- [20] LIU YQ *et al*, *Phys Plasmas* **16** (2009) 056113
- [21] BERKERY J *et al*, *Phys. Rev. Lett.* **104** (2010) 035003
- [22] BERKERY J *et al*, *Phys. Plasmas* **17** (2010) 082504
- [23] LIU YQ, *Nucl Fusion* **50** (2010) 095008
- [24] GRYAZNEVICH MP *et al*, *Plasma Phys. Control. Fusion* **50** 124030 (2008)
- [25] REIMERDES H *et al*, *Phys. Rev. Lett.* **93** (2004) 135002
- [26] MIKHAILOVSKII AB *et al*, *Plasma Phys. Rep.* **23** (1997) 844
- [27] PINCHES SP *et al*, *Comput. Phys. Commun.* **111** (1998) 133 (Release Version 8.09)
- [28] BUDNY RV *et al*, *Nucl. Fusion* **32** (1992) 429
- [29] HUYSMANS GTA, *Plasma Phys Control Fusion* **47** (2005) 2107
- [30] SATO M and NAKAJIMA N, *Phys Plasmas* **13** (2006) 102507
- [31] MATSUNAGA G *et al*, *22nd IAEA FEC, Geneva EX/5-2* (2008)
- [32] OKABAYASHI M *et al*, *22nd IAEA FEC, Geneva EX/P9-5* (2008)
- [33] FITZPATRICK R, *Phys Plasmas* **2** (1995) 825
- [34] GIBSON KJ *et al*, *Plasma Phys. Control. Fusion* submitted 2010

*This work was funded by the RCUK Energy Programme under grant EP/G003955 and the European Communities under the contract of Association between EURATOM and CCFE. The views and opinions expressed herein do not necessarily reflect those of the European Commission.*